Different magneto-optical response of magnetic sublattices as a function of temperature in ferrimagnetic bismuth iron garnet films

Marwan Deb,[1,2,*] Elena Popova,[1] and Niels Keller[1]

[1]*Groupe d'Etude de la Matière Condensée (GEMaC), CNRS-UVSQ, Université Paris-Saclay, 78035 Versailles, France*

[2]*Institut für Physik und Astronomie, Universität Potsdam, Karl-Liebknecht-Strasse 24-25, 14476 Potsdam, Germany*

(Received 8 October 2019; published 12 December 2019)

In this paper we investigate the magneto-optical (MO) and magnetic properties of bismuth iron garnet $Bi_3Fe_5O_{12}$ thin films over a wide range of photon energies (1.6–3.5 eV) and temperatures (5–740 K). Depending on the photon energy range, the Faraday rotation (Θ_F) and ellipticity (ε_F) vary nonmonotonously with temperature. This behavior cannot be explained by a magnetization variation that can only decrease with increasing temperature. Θ_F and ε_F spectra have therefore been analyzed using a model based on two optical transitions of a diamagnetic nature, representing the tetrahedral and octahedral iron sites. Thus, the contribution of each magnetic sublattice has been extracted from the global macroscopic MO response and investigated as a function of temperature. The magnetic properties of octahedral and tetrahedral sublattices depend differently on temperature, suggesting a different anisotropy due to oxygen coordination. We have demonstrated that this relatively simple macroscopic measurement with a subsequent analysis can grant access to the information on the properties at a microscopic level. These results can advance the fundamental understanding of MO properties in multisublattice magnetic materials.

DOI: 10.1103/PhysRevB.100.224410

I. INTRODUCTION

Since their first synthesis by Bertaut and Forrat in 1956 [1], ferrimagnetic and insulating iron garnets have always been the subject of extensive research for both fundamental science and technological applications [2–4]. This continuous interest in garnets is due to their wide variety of exotic and useful physical properties at room temperature, such as low magnetic damping [5], excellent magneto-optical (MO) Faraday activity [6], good magnetoacoustic coupling [7,8], large photomagnetic effects [9], adjustable electrical conductivity [10], and magnetoelectric coupling [11,12]. In recent years, iron garnets are still being investigated for important and often unexpected phenomena in several modern fields of condensed matter physics, such as femtomagnetism [13,14], spintronics [4,15], magnonics [16,17], picomagnetoacoustics [18–20], as well as in the field of photonics [21,22]. A key feature behind the capability to exhibit this wide range of functionalities is related to the complexity of the garnet structure together with its chemical flexibility [2,3]. Indeed, iron garnets have the $Ia\bar{3}d$ space group with an elementary unit cell containing eight $\{R_3\}[Fe_2](Fe_3)O_{12}$ formula units where { }, [ ], and ( ) represent the dodecahedral, octahedral, and tetrahedral sites, respectively, and R can be yttrium, rare earth, or another ion such as bismuth. The nature of the ions in dodecahedral sites defines several important properties of iron garnets, such as, for example, magnetic damping, compensation temperature (T_{comp}), and MO effects [2,3]. On the other hand, the doping of the tetrahedral and/or octahedral sites with ions of different magnetic and/or electron valence (Al^{3+}, Ca^{2+}, Ga^{3+}, Mn^{3+}, Si^{4+}, Co^{2+}, etc.) can be used to tune magnetic and electric properties including T_C, T_{comp}, magnetic anisotropy [2,3], and conductivity [10], or to induce new functionalities such as the photomagnetic effects [9,23].

One of the most important properties of iron garnets is the huge enhancement of the MO Faraday effects in the visible and near infrared region with increasing Bi concentration [3,6]. This enhancement is accompanied by the good transparency characterizing iron garnets (band gap $E_g \sim 2.5$ eV), which makes Bi-substituted iron garnets (Bi-IG) promising candidates for nonreciprocal MO devices. Indeed, Bi-IG and completely Bi-substituted iron garnets ($Bi_3Fe_5O_{12}$, BIG) have been used to fabricate high performing optical circulators and optical isolators for photonic and optoelectronic integrated circuits [24–26]. From a fundamental point of view, there are two aspects of the enhancement of MO effects that are of great interest. The first is related to the understanding of the origin of this phenomenon. From a microscopic point of view, a large spin-orbit coupling induced in Fe-3d orbitals due to their hybridization with Bi-6p ones was used by Wittekoek *et al.* [27] to explain such an enhancement. This mechanism was later supported theoretically by cluster molecular-orbital theory [28,29] and band-structure calculations [30]. On the other hand, Dionne and Allen have proposed to describe the influence of Bi on MO spectra with a model based on optical transitions of a diamagnetic nature, which are related to the crystal energy levels of Fe^{3+} ions in tetrahedral an octahedral sublattices [31,32]. This model has been widely used to analyze the MO spectra [33–36]. However, most of the previous investigations were carried out at room temperature and in a limited range of photon energy [33–35]. The second aspect is related to almost the entire the above-mentioned modern field of research exploring physical properties and new phenomena

*Corresponding author: madeb@uni-potsdam.de

in iron garnets. Indeed, since light provides important and unique opportunities to probe ultrafast magnetic processes with a very high spatiotemporal resolution using femtosecond MO pump-probe spectroscopy techniques, MO properties of the studied garnets are usually enhanced by a Bi substitution in order to detect magnetic phenomena in the most efficient way [18–20,37–45]. In these two main contexts, it is therefore very important to study in detail the MO properties in BIG in order to understand and control them as a function of temperature and photon energy.

The aim of the present paper is to investigate in detail the MO and magnetic properties of BIG. Toward this goal, we measured the Faraday rotation and ellipticity spectra over a broad range of photon energies (1.6–3.5 eV) and temperatures (5–740 K). By analyzing the results using a simple model based on two optical transitions of a diamagnetic nature, representing the tetrahedral and octahedral iron sites, we extracted the individual contribution of each sublattice from the global MO response and we tracked their properties as a function of temperature. We demonstrate that the two iron sublattices possess different MO and magnetic behavior as a function of temperature and photon energy. These unequal behaviors allow us to explain all features characterizing the MO spectra and their temperature dependence.

II. SAMPLE AND EXPERIMENTAL METHODS

The sample used in this study is 220-nm-thick BIG film, grown onto a (100) gadolinium gallium garnet ($Gd_3Ga_5O_{12}$, GGG) substrate by pulsed laser deposition (PLD). The used PLD setup is equipped with a reflection high-energy electron diffraction (RHEED) and ellipsometry system allowing a real time characterization of the structural and optical properties during the sample growth. The BIG target is prepared by a standard ceramic processing method and has a slight excess of bismuth (the Bi/Fe ratio was 0.63) to compensate the cation loss during ablation due to bismuth volatility. The target is ablated using pulses generated by a KrF laser operating at a 1-kHz repetition rate and delivering 20-ns pulses centered at 248 nm. The laser energy density is kept constant at $2.1\,J/cm^2$. The sample growth is performed at 950 K in a stable oxygen pressure. After the deposition, the sample is cooled down in the growth atmosphere. The above-described growth process yields single-crystalline and single-phase BIG films as confirmed by *ex situ* x-ray diffraction and transmission electron microscopy [46]. On the other hand, we note that a detailed investigation of the optical properties of BIG films with a similar thickness can be found in Ref. [36].

The study of the MO properties was carried out in a polar Faraday configuration using a custom designed broadband MO spectrometer based on a 90°-polarization modulation technique. Briefly, the white light emitted by a 100-W Hg arc lamp is polarized by a Glan-Taylor prism and modulated at a high frequency of 50 kHz by a Hinds photoelectric modulator (PEM). The modulated light is focused onto the sample at normal incidence. The transmitted light is collimated then analyzed with a Glan-Taylor prism and focused into a monochromator to select the desired photon energy E_{ph}. The Faraday rotation (Θ_F) and ellipticity (ε_F) are simultaneously recorded

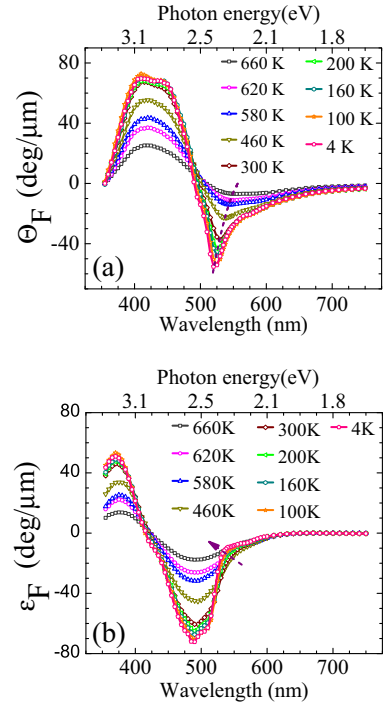

FIG. 1. Temperature dependence of the (a) Θ_F and (b) ε_F spectra of the BIG thin film. The dashed line in (a) and the arrow in (b) are guides to the eye.

from the signal measured by a photomultiplier detector and injected into two lock-in amplifiers referenced to the first and second harmonics of the PEM. For variable-temperature measurements, the sample was mounted consecutively in a standard helium-flow cryostat and an optical furnace, which allow efficient thermal control of the sample temperature from 5 K up to 1000 K. The spectral dependency of Θ_F (respectively ε_F) is obtained at each selected temperature from the difference between the Θ_F (respectively ε_F) spectra measured for positive and negative saturating external magnetic fields of $H_{ext} = \pm 1.3\,T$ using the following equation, $X_F = [X(H^+) - X(H^-)]/2$, with $X = (\Theta, \varepsilon)$. This avoids any contribution that is not proportional to the magnetization in the MO spectra [47]. We mention that the MO background induced by the glass windows of the cryostat or the furnace and the paramagnetic GGG substrate has been also measured at each temperature and their contributions have been carefully subtracted in order to obtain the intrinsic MO spectra of BIG.

III. RESULTS AND DISCUSSION

Figure 1 displays the temperature dependence of Θ_F [Fig. 1(a)] and ε_F [Fig. 1(b)] spectra measured over a wide range of photon energies (1.6–3.5 eV) at selected temperatures between 5 and 660 K. The spectral dependencies of both Θ_F and ε_F at 300 K are in good agreement with previous investigations of room-temperature MO properties of BIG: Θ_F is negative below 2.5 eV and positive between 2.5 and 3.5 eV with a maximum near 3 eV, whereas ε_F has two peaks centered at 2.52 and 3.34 eV [36,40,48]. On the other hand,

two important features are observed in the temperature dependence of the MO spectra. The first is the clear difference in the behavior of the two peaks in the Θ_F spectra. Indeed, while the peak with a negative sign shows a blueshift and narrowing with decreasing temperature, the one with a positive sign occurs at the same photon energy [see Fig. 1(a)]. In addition, in the temperature range 100–300 K, the amplitude of the negative peak increases by about 50% while the one with a positive sign is almost independent of temperature. We mention that the peak positions of the ε_F spectra are independent of temperature, while their amplitudes show the same behavior as for Θ_F [see Fig. 1(b)]. The second important feature is observed in ε_F spectra between 2.1 and 2.38 eV, where the amplitude of ε_F continuously decreases with decreasing temperature from 300 to 100 K [see Fig. 1(b)]. Such decreases cannot be explained by the simple proportionality of MO effects to the magnetization, which in BIG can only increase when the temperature decreases.

In order to understand these complex behaviors of MO spectra as a function of temperature, we analyzed the spectral dependence of Θ_F and ε_F in the framework of the model developed by Dionne *et al.* [31,32] in order to describe the influence of Bi on the MO properties in Bi-IG. For a photon energy range between 1.6 and 3.5 eV, this model is described by two optical transitions of a diamagnetic nature representing the tetrahedral and octahedral sublattices [31,32]. From a fundamental point of view, these absorption lines are associated with the crystal field energy transitions between the ground state $^6A_{1g}$ (^6S) and the second excited state $^4T_{1g}$ (^4P) of Fe^{3+} ions in the two iron sublattices [31,32]. On the other hand, in the framework of this model, the analytic expressions of Θ_F and ε_F spectra are given by

$$\Theta_F(\omega) = \frac{\pi e^2 \omega^2}{2nmc} \sum_{i=a,d} \left[\frac{N_i f_i}{\omega_{0i}} \left\{ \frac{(\omega_{0i}+\Delta_i)^2 - \omega^2 - \Gamma_i^2}{\left[(\omega_{0i}+\Delta_i)^2 - \omega^2 + \Gamma_i^2\right]^2 + 4\omega^2\Gamma_i^2} - \frac{(\omega_{0i}-\Delta_i)^2 - \omega^2 - \Gamma_i^2}{\left[(\omega_{0i}-\Delta_i)^2 - \omega^2 + \Gamma_i^2\right]^2 + 4\omega^2\Gamma_i^2} \right\} \right], \tag{1}$$

$$\varepsilon_F(\omega) = \frac{\pi e^2 \omega}{2nmc} \sum_{i=a,d} \left[\frac{N_i f_i \Gamma_i}{\omega_{0i}} \left\{ \frac{(\omega_{0i}+\Delta_i)^2 + \omega^2 + \Gamma_i^2}{\left[(\omega_{0i}+\Delta_i)^2 - \omega^2 + \Gamma_i^2\right]^2 + 4\omega^2\Gamma_i^2} - \frac{(\omega_{0i}-\Delta_i)^2 + \omega^2 + \Gamma_i^2}{\left[(\omega_{0i}-\Delta_i)^2 - \omega^2 + \Gamma_i^2\right]^2 + 4\omega^2\Gamma_i^2} \right\} \right]. \tag{2}$$

The summation comprises the contributions of both tetrahedral ($i = a$) and octahedral ($i = d$) sublattices. m and e correspond to the electron charge and mass, f_i is the oscillator strength, ω_{0i} represents the resonant energy of the optical transition, Δ_i is the spin-orbit splitting energy, Γ_i is the linewidth, ω is the frequency of probing light, and n is the refractive index of bismuth iron garnet. This model still requires the collinearity of the N_i magnetic moments (transition centers), which occurs through both the external and the exchange field. The degree of collinearity follows a Brillouin function. Hence, the effective number of transition centers can be described by $N_i = N_{i0}\ B_i(H, T)$, where N_{i0} are the zero-temperature transition centers in each sublattice.

In order to reproduce the experimental data with the model, we first started by fitting the Θ_F and ε_F spectra measured at 300 K using as initial parameter set for Δ_i, ω_{0i}, Γ_i the values of Ref. [36], which are determined for BIG at room temperature and demonstrated to be thickness independent. We also used in all our analysis a refractive index of $n(E_{\rm ph}) = 2.51 + (E_{\rm ph}/3.75)^2$, which is obtained for BIG film with the same thickness [36]. The product $N_i f_i$ is chosen as a free parameter. After the fitting procedure, we find that the Θ_F and ε_F spectra are simultaneously reproduced with an almost identical parameter set as Ref. [36]. We then fitted the MO spectra measured at the other temperatures. Taking into account that (i) the spin-orbit splitting Δ_i is induced by the large Bi^{3+} spin-orbit interaction [27–32] together with (ii) the high stability characterizing the garnet structure in the studied temperature range (e.g., no structural transition occurs to the cubic lattice) [2,3], we have reasonably assumed in these fits that Δ_i is temperature independent. We therefore maintained Δ_i for all temperatures of $\Delta_{\rm tetra} = 0.076$ eV and $\Delta_{\rm octa} = 0.4$ eV, as obtained at 300 K. The parameters ω_{0i}, Γ_i, and $N_i f_i$ extracted from the fits and their temperature dependence will be discussed below in detail.

Figure 2 displays the theoretical descriptions of the MO properties at two selected temperatures of 660 K [Figs. 2(a) and 2(c)] and 5 K [Figs. 2(b) and 2(d)], which show good agreement with the experimental data. A major advantage of the theoretical analysis is that it allows determining the individual contribution of each Fe^{3+} sublattice in the global MO response. The contributions of the tetrahedral and octahedral sublattices are plotted in Fig. 2 by the dashed and dashed-dotted lines, respectively. They show two important features. First, both Θ_F and ε_F responses come mainly from the octahedral sublattice in the energy range above 3 eV where the MO effects slightly depend on temperature below 300 K. Second, the contribution of the tetrahedral sublattice to the MO effect is significant in the photon energy range characterized by a strong variation of Θ_F and ε_F between 300 and 100 K. Based on the above description of the temperature dependence of Θ_F and ε_F spectra (Fig. 1) and their theoretical analysis (Fig. 2), it is obvious that the MO contribution of the tetrahedral sublattice ($E_{\rm ph} \sim 2.5$ eV) has a different thermal variation compared to the one of the octahedral sublattice ($E_{\rm ph} \sim 2.9$ eV).

It is worth emphasizing here that near the peak at low energy in both Θ_F and ε_F spectra the contributions of tetrahedral and octahedral sublattices have the same sign, whereas the peak at high energy is highly dominated by the contribution of the octahedral site (i.e., tetrahedral contribution ~0). In these cases, MO intensity progressively increases when the temperature increases until it becomes almost constant below 100 K. On the other hand, when the contributions of the two sublattices have a similar amplitude but opposite signs, a decrease of the MO effect can occur when the temperature decreases,

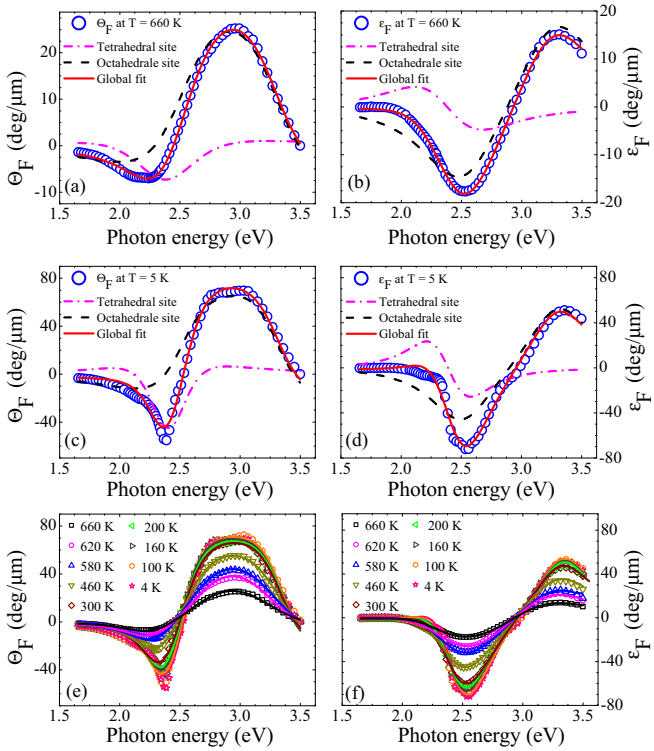

FIG. 2. (a)–(d) Experiential measurement (symbols) and theoretical simulation (solid lines) of (a), (c) Θ_F and (c), (d) ε_F spectra for two selected temperatures of $T = 5$ and 660 K. The dashed and the dashed-dotted lines represent the contribution from the tetrahedral and octahedral diamagnetic electric dipole transitions. (e), (f) Comparison of experimental (symbols) and theoretical simulation (solid lines) of Θ_F and ε_F spectra obtained at various temperatures.

as can be clearly seen for ε_F near 2.25 eV [Fig. 2(b)]. We note that the same phenomenon also occurs in Θ_F near 2.5 eV [Fig. 2(a)]. Importantly, we note that the observation of this effect should require, in addition to the opposite sign of the two sublattice contributions, that their contributions change differently with temperature.

Let us now discuss the temperature dependence of the parameters ω_{0i}, Γ_i, and $N_i f_i$. The transition energy ω_{0i} shows no temperature dependence in both iron sublattices (see Fig. 3). This is in good agreement with the high stability of the garnet structure in the investigated temperature range [2,3]. It also supports our assumption concerning the temperature-independent spin-orbit splitting in BIG. By taking into consideration the results in the literature, it can be concluded that ω_{0i} is more affected by bismuth stoichiometry [36,48,49] than by thickness [36] or temperature. Contrary to ω_{0i}, Γ_i and $N_i f_i$ are highly temperature dependent (see Fig. 4). Indeed, with decreasing temperature from 660 to 5 K, Γ_i significantly decreases by 45% and 22%, respectively, for the tetrahedral and octahedral sublattices [Fig. 4(a)]. This behavior of Γ_i is associated with narrowing of the peaks in the MO spectra when the temperature decreases, as shown in Fig. 1. On the other hand, for both sublattices, the product $N_i f_i$ increases with decreasing temperature [Fig. 4(b)]. To discuss further this result, let us first note that for MO effects induced by

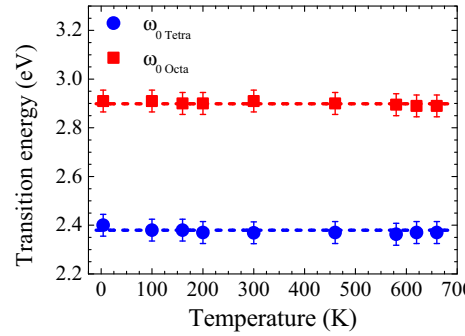

FIG. 3. Temperature dependence of the energy transition ω_{0i} characterizing the tetrahedral (circle) and octahedral (square) diamagnetic electric dipole transitions. The dashed lines are guides to the eye.

diamagnetic lines, the density of transition centers N_i for each sublattice should be directly proportional to its magnetization. Therefore, by assuming that f_i is temperature independent, the ratio of the product $N_i f_i$ at two different temperatures should have the same ratio as the magnetization M_i of its related sublattice. The calculated ratios of magnetization between 5 and 300 K are therefore of $M_{\text{tetra}}(5\,\text{K})/M_{\text{tetra}}(300\,\text{K}) = 1.23$ and $M_{\text{octa}}(5\,\text{K})/M_{\text{octa}}(300\,\text{K}) = 1.05$ for the tetrahedral and octahedral sublattices, respectively. This result clearly indicates that below 300 K the magnetization amplitude of

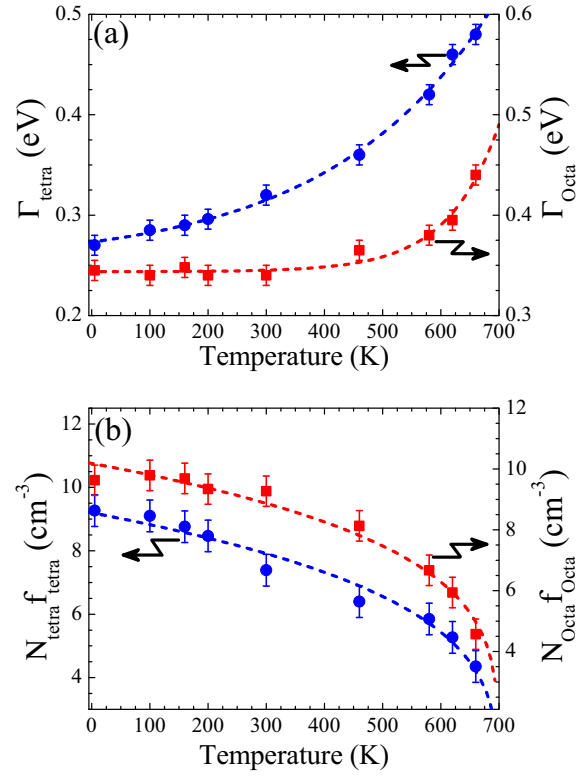

FIG. 4. Temperature dependence of the half linewidth Γ_i and the $N_i f_i$ parameters characterizing the tetrahedral (circle) and octahedral (square) diamagnetic electric dipole transitions. For better visualization, the scales on the left and right axis are different. The dashed lines are guides to the eye.

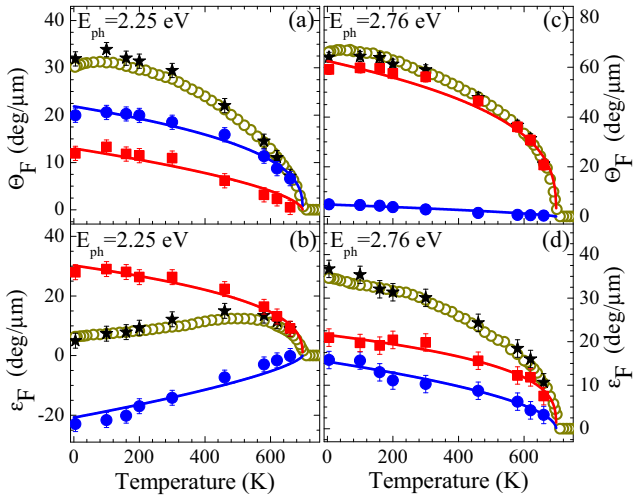

FIG. 5. Temperature dependence of the (a), (c) Θ_F and (b), (d) ε_F measured at photon energies of 2.25 and 2.76 eV (open circles). The solid circles and squares represent the temperature dependence of the contribution of the tetrahedral and octahedral sublattices, respectively. The stars represent the sum of the contributions of the two sublattices. The solid lines are guides to the eye.

the tetrahedral sublattice changes more with temperature than the one of the octahedral sublattice. It also confirms the results of Scott *et al.* [50] showing that in yttrium iron garnet ($Y_3Fe_5O_{12}$) $M_{\text{tetra}}(77\,\text{K})/M_{\text{tetra}}(300\,\text{K}) = 1.19$ and $M_{\text{octa}}(77\,\text{K})/M_{\text{octa}}(300\,\text{K}) = 1.12$. By taking into account the different contributions of the Fe^{3+} sublattices in the MO spectra (see Fig. 2), the behavior of the magnetization in the two sublattices is in agreement with the different temperature dependences of the negative and positive peaks observed in Θ_F and ε_F spectra below 300 K.

In order to study in more detail the MO and magnetic properties of BIG, we have also directly measured the temperature dependence of Θ_F and ε_F at two selected phonon energies of $E_{\text{ph}} = 2.25$ and 2.76 eV and compared the results with the theoretical prediction deduced from the analyses of MO spectra (see Fig. 5). Let us first note that a good agreement between the direct measurements and theoretical prediction is observed for both $\Theta_F(T)$ and $\varepsilon_F(T)$ at the two E_{ph}. On the other hand, despite the complex behavior of $\varepsilon_F(T)$ measured at $E_{\text{ph}} = 2.25\,\text{eV}$, which does not follow a Brillouin function, we find that the temperature dependence of the tetrahedral and octahedral contributions follows a Brillouin function for both Θ_F and ε_F as well as at the two E_{ph}. Using the results of the theoretical analysis, the Brillouin behavior of each sublattice contribution is confirmed for all E_{ph} between 1.6 and 3.5 eV. Furthermore, we also show here that below 300 K the relative contribution of the tetrahedral sublattice changes more than the one of an octahedral sublattice. This characteristic behavior is at the origin of the very complex temperature dependence of the MO effect when the contributions of the two sublattices have opposite signs [Fig. 5(b)]. Indeed, we have checked for several different E_{ph} that the observation of a complex temperature dependence of Θ_F and ε_F [i.e., similar to the one observed in Fig. 5(b)] occurs only when the contributions of the two sublattices have opposite signs. We believe that this result can be generalized to any ferrimagnetic material in the following way: The observation of an increase of a MO effect when the temperature increases reveals that the MO contributions related to the different magnetic sublattices have opposite signs and their amplitude changes differently as a function of temperature.

IV. CONCLUSION

We have studied MO and magnetic properties in the ferrimagnetic insulator $Bi_3Fe_5O_{12}$ over a wide range of photon energies (1.6–3.5 eV) and temperatures (5–740 K). We analyzed the experimental Θ_F and ε_F spectra measured at different temperatures using a model based on two diamagnetic lines associated with tetrahedral and octahedral sublattices, which allows us to extract the individual contribution of each sublattice from the global MO response and track their related properties as a function of temperature. We have clearly demonstrated the unequal MO and magnetic behavior of tetrahedral and octahedral sublattices. In particular, we proved that the magnetization, Faraday rotation, and ellipticity amplitudes related to the tetrahedral sublattice highly change between 100 and 300 K compared to the ones related to the octahedral sublattices. This property is reflected, when the contributions of the two sublattices have opposite signs, by a complex temperature dependence of the MO effects, which do not follow a Brillouin function. Different oxygen coordination leads to different magnetic anisotropy of the tetrahedral and octahedral sites. These results show the possibility to obtain microscopic-level information from macroscopic measurements and can advance the fundamental understanding of the MO properties in multisublattice magnetic materials.

ACKNOWLEDGMENT

M.D. acknowledges the Alexander von Humboldt Foundation for financial support.

[1] F. Bertaut and F. Forrat, Structure des ferrites ferrimagnetiques des terres rares, C. R. Acad. Sci., Paris **242**, 382 (1956).
[2] G. D. Winkler, *Magnetic Garnets* (Vieweg, Braunschweig, 1981).
[3] G. F. Dionne, *Magnetic Oxides* (Springer, New York, 2009).
[4] A. Willoughby, P. Capper, and S. Kasap, *Spintronics for Next Generation Innovative Devices* (Wiley, Hoboken, NJ, 2015).
[5] A. G. Gurevich and G. A. Melkov, *Magnetization Oscillations and Waves* (CRC Press, Boca Raton, FL, 1996).
[6] P. Hansen and J. P. Krumme, Magnetic and magneto-optical properties of garnet-films, Thin Solid Films **114**, 69 (1984).
[7] E. G. Spencer and R. C. LeCraw, Magnetoacoustic Resonance in Yttrium Iron Garnet, Phys. Rev. Lett. **1**, 241 (1958).
[8] O. Y. Belyaeva, S. N. Karpachev, and L. K. Zarembo, Magnetoacoustics of ferrites and magnetoacoustic resonance, Sov. Phys. - Usp. **35**, 106 (1992).

[9] A. Stupakiewicz, A. Maziewski, I. Davidenko, and V. Zablotskii, Light-induced magnetic anisotropy in Co-doped garnet films, Phys. Rev. B **64**, 064405 (2001).

[10] A. Teurtrie, E. Popova, I. Koita, E. Chikoidze, N. Keller, A. Gloter, and L. Bocher, Atmosphere-induced reversible resistivity changes in Ca/Y-doped bismuth iron garnet thin films, Adv. Funct. Mater. **29**, 1904958 (2019).

[11] Y. Kohara, Y. Yamasaki, Y. Onose, and Y. Tokura, Excess-electron induced polarization and magnetoelectric effect in yttrium iron garnet, Phys. Rev. B **82**, 104419 (2010).

[12] E. Popova, A. Shengelaya, D. Daraselia, D. Japaridze, S. Cherifi-Hertel, L. Bocher, A. Gloter, O. Stéphan, Y. Dumont, and N. Keller, Bismuth iron garnet BiFeO: A room temperature magnetoelectric material, Appl. Phys. Lett. **110**, 142404 (2017).

[13] A. H. M. Reid, A. V. Kimel, A. Kirilyuk, J. F. Gregg, and T. Rasing, Optical Excitation of a Forbidden Magnetic Resonance Mode in a Doped Lutetium-Iron-Garnet Film via the Inverse Faraday Effect, Phys. Rev. Lett. **105**, 107402 (2010).

[14] C. S. Davies, K. H. Prabhakara, M. D. Davydova, K. A. Zvezdin, T. B. Shapaeva, S. Wang, A. K. Zvezdin, A. Kirilyuk, T. Rasing, and A. V. Kimel, Anomalously Damped Heat-Assisted Route for Precessional Magnetization Reversal in an Iron Garnet, Phys. Rev. Lett. **122**, 027202 (2019).

[15] J. Kimling, G.-M. Choi, J. T. Brangham, T. Matalla-Wagner, T. Huebner, T. Kuschel, F. Yang, and D. G. Cahill, Picosecond Spin Seebeck Effect, Phys. Rev. Lett. **118**, 057201 (2017).

[16] S. Klingler, V. Amin, S. Geprägs, K. Ganzhorn, H. Maier-Flaig, M. Althammer, H. Huebl, R. Gross, R. D. McMichael, M. D. Stiles, S. T. B. Goennenwein, and M. Weiler, Spin-Torque Excitation of Perpendicular Standing Spin Waves in Coupled YIG/Co Heterostructures, Phys. Rev. Lett. **120**, 127201 (2018).

[17] M. Deb, E. Popova, M. Hehn, N. Keller, S. Petit-Watelot, M. Bargheer, S. Mangin, and G. Malinowski, Femtosecond Laser-Excitation-Driven High Frequency Standing Spin Waves in Nanoscale Dielectric Thin Films of Iron Garnets, Phys. Rev. Lett. **123**, 027202 (2019).

[18] M. Deb, E. Popova, M. Hehn, N. Keller, S. Mangin, and G. Malinowski, Picosecond acoustic-excitation-driven ultrafast magnetization dynamics in dielectric Bi-substituted yttrium iron garnet, Phys. Rev. B **98**, 174407 (2018).

[19] Y. Hashimoto, S. Daimon, R. Iguchi, Y. Oikawa, K. Shen, K. Sato, D. Bossini, Y. Tabuchi, T. Satoh, B. Hillebrands, G. E. W. Bauer, T. H. Johansen, A. Kirilyuk, T. Rasing, and E. Saitoh, All-optical observation and reconstruction of spin wave dispersion, Nat. Commun. **8**, 15859 (2017).

[20] Y. Hashimoto, D. Bossini, T. H. Johansen, E. Saitoh, A. Kirilyuk, and T. Rasing, Frequency and wavenumber selective excitation of spin waves through coherent energy transfer from elastic waves, Phys. Rev. B **97**, 140404(R) (2018).

[21] L. Bi, J. Hu, P. Jiang, D. H. Kim, G. F. Dionne, L. C. Kimerling, and C. A. Ross, On-chip optical isolation in monolithically integrated non-reciprocal optical resonators, Nat. Photon. **5**, 758 (2011).

[22] R. R. Subkhangulov, R. V. Mikhaylovskiy, A. K. Zvezdin, V. V. Kruglyak, T. Rasing, and A. V. Kimel, Terahertz modulation of the Faraday rotation by laser pulses via the optical Kerr effect, Nat. Photon. **10**, 111 (2016).

[23] A. Stupakiewicz, K. Szerenos, D. Afanasiev, A. Kirilyuk, and A. V. Kimel, Ultrafast nonthermal photo-magnetic recording in a transparent medium, Nature (London) **542**, 71 (2017).

[24] M. Levy, The on-chip integration of magnetooptic waveguide isolators, IEEE J. Sel. Top. Quantum Electron. **8**, 1300 (2002).

[25] L. Magdenko, E. Popova, M. Vanwolleghem, C. Pang, F. Fortuna, T. Maroutian, P. Beauvillain, N. Keller, and B. Dagens, Wafer-scale fabrication of magneto-photonic structures in bismuth iron garnet thin film, Microelectron. Eng. **87**, 2437 (2010).

[26] B. J. H. Stadler and T. Mizumoto, Integrated magneto-optical materials and isolators: A review, IEEE Photonics J. **6**, 1 (2014).

[27] S. Wittekoek and D. E. Lacklison, Investigation of the Origin of the Anomalous Faraday Rotation of $Bi_xCa_{3-x}Fe_{3.5+0.5x}V_{1.5-0.5x}O_{12}$ by Means of the Magneto-optical Kerr Effect, Phys. Rev. Lett. **28**, 740 (1972).

[28] A. V. Zenkov and A. S. Moskvin, Bismuth-induced increase of the magneto-optical effects in iron garnets: A theoretical analysis, J. Phys.: Condens. Matter **14**, 6957 (2002).

[29] S. Sugano and N. Kojima, *Magneto-Optics* (Springer, Berlin, 2013).

[30] T. Oikawa, S. Suzuki, and K. Nakao, First-principles study of spin-orbit interactions in bismuth iron garnet, J. Phys. Soc. Jpn. **74**, 401 (2005).

[31] G. A. Allen and G. F. Dionne, Application of permittivity tensor for accurate interpretation of magneto-optical spectra, J. Appl. Phys. **73**, 6130 (1993).

[32] G. F. Dionne and G. A. Allen, Molecular-orbital analysis of magneto-optical Bi-O-Fe hybrid excited states, J. Appl. Phys. **75**, 6372 (1994).

[33] L. E. Helseth, R. W. Hansen, E. I. Il'yashenko, M. Baziljevich, and T. H. Johansen, Faraday rotation spectra of bismuth-substituted ferrite garnet films with in-plane magnetization, Phys. Rev. B **64**, 174406 (2001).

[34] L. E. Helseth, A. G. Solovyev, R. W. Hansen, E. I. Il'yashenko, M. Baziljevich, and T. H. Johansen, Faraday rotation and sensitivity of (100) bismuth-substituted ferrite garnet films, Phys. Rev. B **66**, 064405 (2002).

[35] S. Kahl, V. Popov, and A. M. Grishin, Optical transmission and Faraday rotation spectra of a bismuth iron garnet film, J. Appl. Phys. **94**, 5688 (2003).

[36] M. Deb, E. Popova, A. Fouchet, and N. Keller, Magneto-optical Faraday spectroscopy of completely bismuth-substituted $Bi_3Fe_5O_{12}$ garnet thin films, J. Phys. D: Appl. Phys. **45**, 455001 (2012).

[37] F. Hansteen, A. Kimel, A. Kirilyuk, and T. Rasing, Femtosecond Photomagnetic Switching of Spins in Ferrimagnetic Garnet Films, Phys. Rev. Lett. **95**, 047402 (2005).

[38] F. Hansteen, A. Kimel, A. Kirilyuk, and T. Rasing, Nonthermal ultrafast optical control of the magnetization in garnet films, Phys. Rev. B **73**, 014421 (2006).

[39] S. Parchenko, A. Stupakiewicz, I. Yoshimine, T. Satoh, and A. Maziewski, Wide frequencies range of spin excitations in a rare-earth Bi-doped iron garnet with a giant Faraday rotation, Appl. Phys. Lett. **103**, 172402 (2013).

[40] M. Deb, M. Vomir, J.-L. Rehspringer, and J.-Y. Bigot, Ultrafast optical control of magnetization dynamics in polycrystalline bismuth doped iron garnet thin films, Appl. Phys. Lett. **107**, 252404 (2015).

[41] N. Ogawa, W. Koshibae, A. J. Beekman, N. Nagaosa, M. Kubota, M. Kawasaki, and Y. Tokura, Photodrive of magnetic bubbles via magnetoelastic waves, Proc. Natl. Acad. Sci. USA **112**, 8977 (2015).

[42] M. Deb, P. Molho, B. Barbara, and J.-Y. Bigot, Temperature and magnetic field dependence of rare-earth↔iron exchange resonance mode in a magnetic oxide studied with femtosecond magneto-optical Kerr effect, Phys. Rev. B **94**, 054422 (2016).

[43] S. Parchenko, T. Satoh, I. Yoshimine, F. Stobiecki, A. Maziewski, and A. Stupakiewicz, Non-thermal optical excitation of terahertz-spin precession in a magneto-optical insulator, Appl. Phys. Lett. **108**, 032404 (2016).

[44] M. Deb, P. Molho, B. Barbara, and J.-Y. Bigot, Controlling laser-induced magnetization reversal dynamics in a rare-earth iron garnet across the magnetization compensation point, Phys. Rev. B **97**, 134419 (2018).

[45] M. Jäckl, V. I. Belotelov, I. A. Akimov, I. V. Savochkin, D. R. Yakovlev, A. K. Zvezdin, and M. Bayer, Magnon Accumulation by Clocked Laser Excitation as Source of Long-Range Spin Waves in Transparent Magnetic Films, Phys. Rev. X **7**, 021009 (2017).

[46] E. Popova, M. Deb, L. Bocher, A. Gloter, O. Stéphan, B. Warot-Fonrose, B. Berini, Y. Dumont, and N. Keller, Interplay between epitaxial strain and low dimensionality effects in a ferrimagnetic oxide, J. Appl. Phys. **121**, 115304 (2017).

[47] M. Deb, E. Popova, A. Fouchet, and N. Keller, Full spin polarization of complex ferrimagnetic bismuth iron garnet probed by magneto-optical Faraday spectroscopy, Phys. Rev. B **87**, 224408 (2013).

[48] C. Ming-Yau, L. Fang-Yuh, L. Da-Ren, Y. Kuang, and L. Juin-Sen, Red shift of Faraday rotation in thin films of completely bismuth-substituted iron garnet $Bi_3Fe_5O_{12}$, Jpn. J. Appl. Phys. **38**, 6687 (1999).

[49] B. Vertruyen, R. Cloots, J. S. Abell, T. J. Jackson, R. C. da Silva, E. Popova, and N. Keller, Curie temperature, exchange integrals, and magneto-optical properties in off-stoichiometric bismuth iron garnet epitaxial films, Phys. Rev. B **78**, 094429 (2008).

[50] G. B. Scott, D. E. Lacklison, and J. L. Page, The effect of octahedral Fe^{3+} and tetrahedral Fe^{3+} dilution on the Faraday spectra of bismuth-doped iron garnets, J. Phys. C: Solid State Phys. **8**, 519 (1975).